Influence of sand liquefaction on the self-burial of a pipe submitted to wave action

Pierre Foray, D. Bonjean, Hervé Michallet

Influence of Sand Liquefaction on Self-burial of a Pipe Subject to Wave Action

P. Y. Foray and D. Bonjean
Laboratory 3S, Institut National Polytechnique de Grenoble, Grenoble, France

H. Michallet
LEGI (CNRS-INPG-UJF), Grenoble, France

Coastal or offshore structures such as pipelines installed on the seabed are subject to cyclic horizontal loads either by direct hydrodynamic wave action or through the cyclic movement of risers or flow lines transmitted by floating structures. In fine sandy or silty soils, such cyclic loads may lead to liquefaction of the surrounding bed, which can play an important part in the processes of erosion, trenching or self-burial of the pipes. A large 1-g physical model was built to study the fluid-soil-structure interaction, with special emphasis placed on the conditions in which liquefaction occurs around a pipe instrumented with pore-pressure transducers. The experiments indicate a strong increase in pore pressure at the pipe-soil interface, and lateral visualization revealed the liquefaction of a soil band in the vicinity of the pipe. The penetration of the structure can be related to the phenomenon of liquefaction.

INTRODUCTION

The process of self-burial of structures resting on the seabed as a result of wave action has been extensively studied by Lyons (1973), Lambrakos (1985), Brennoden et al. (1986), Wagner et al. (1987), Palmer et al. (1988) and Morris et al. (1988), among others. Many of these studies were devoted to specific pipe-soil interaction in order to draw up design criteria for pipeline stability. The first experimental program was conducted at the University of Grenoble by Branque et al. (2001, 2002) to quantify the influence of cyclic amplitude and sand density on pipe penetration and changes in lateral resistance. Transitory liquefaction of the soil close to the pipe was noted in some of the tests, with peak cyclic pore pressures reaching the effective overburden stress.

In recent years, increasing attention has been paid to the effect on the stability of coastal or offshore structures of wave-induced liquefaction, in combination with scour effects. Field observations indicate that liquefaction can play an important part in erosion and stability problems for breakwaters or pipelines. Theoretical approaches have been devoted to the conditions of occurrence of seabed liquefaction due to the cyclic shear loading induced by waves (Sumer et al., 1999; Sassa et al., 2001; Cheng et al., 2001). Within the framework of the European program LIMAS (Liquefaction Around Marine Structures), experimental studies were conducted in sand flumes with buried pipes by Sumer et al. (2005a, b); Teh et al. (2003) focused on the effect of liquefaction of the entire seabed on pipeline sinking or flotation. Within the same program, a series of tests was performed at the University of Grenoble, oriented towards the study of fluid-soil-structure interaction, emphasizing pore-pressure measurements at the pipe-soil interface and within the soil. The conditions of liquefaction occurrence and their effect on pipe stability were studied. The first experimental results are presented here. In most of these tests, the effects of hydrodynamic forces were simulated by applying cyclic loads or displacements on the pipe model. Nevertheless, Damgaard and Palmer (2001) discussed the order of magnitude of the different processes leading to pipe instability and found that the hydrodynamic forces necessary to move a pipe resting on the seabed laterally cause sediment transport and liquefaction before any significant movement of the pipe occurs. Hence such experiments are more representative of the cyclic effects of a floating structure linked to flow lines or risers resting on the seabed.

KEY WORDS: Pore pressure generation, saturation, dense and loose sands, Morison equation, load and displacement controlled tests.

EXPERIMENTAL SETUP

General Settings

The experimental setup constructed at the University of Grenoble by Branque (1998) is similar to the one used in the Pipestab research program undertaken by Brennoden et al. (1986) and Wolfram et al. (1987). In the present research program, large modifications were made to the setup in order to achieve better control of the loading conditions, and to view laterally the liquefaction process around the structure. A rigid tank 2 m long, 1 m wide and 1 m deep is filled with sand. One side of the tank is made of glass, about 1 m $\times$ 1 m, for direct visualization of the deformation in the sand. Fig. 1 gives a general view of the experimental setup.

A trolley supporting a 1-m-long pipeline section can roll on 2 horizontal rails along the length of the tank, parallel to the windows. The pipe itself is free to move vertically between 2 guides and then penetrate the sand under its self-weight. The section of pipe and the glass are connected with a rubber joint, allowing the visualization of a 2-dimensional cross-section of the pipe-soil interaction perpendicular to the pipe axis. It is also possible to make a video of the experiments and show the occurrence of liquefaction.

Pipe Instrumentation

These experiments used a structure consisting of a half-pipe 200 mm in diam and 24 kg/m in mass/unit length. The pipe section was instrumented with 5 Druck PDCR 4030 pore-pressure transducers located on the external surface in contact with the soil. The pore pressure in the soil is transmitted to the transducer through a porous stone fixed at the connection between pipe and transducer. This part was carefully saturated before each test. The

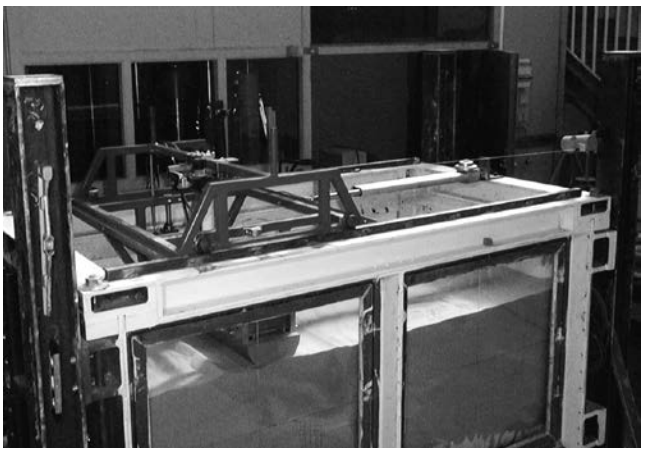

Fig. 1 Experimental setup, with electromechanical actuator set

transducers measure relative pressure up to 7×10^4 Pa with a precision of 0.08%. This corresponds to an accuracy in the water depth of about 0.5 mm. For some tests, pore-pressure transducers were also installed within the seabed, close to the pipe.

Fig. 2 shows the respective positions of the transducers. As it was not possible to install all 5 transducers along the same pipe cross-section, they were fixed on the surface at different sections in the central part of the pipe. It is then assumed that the distribution of excess pore pressure is homogeneous along the pipe's length.

Loading Systems

A mechanical actuator fixed on the tank moves a trolley horizontally. A load cell links the actuator to the trolley. A computer-controlled electrical motor moves the actuator. This setup allows a load-controlled regulation of the actuator in order to reproduce the cyclic wave-induced hydrodynamic forces acting on the pipeline.

An alternative loading system was also used in order to perform displacement-controlled tests. A crankshaft-connecting rod system converts a circular motor motion into a horizontal sinusoidal movement. Such a device does not prevent load-controlled regulation of the movement, but it does allow much more accurate control of pipe displacement. Although such loading conditions do not exactly represent the hydrodynamic effects, they are of interest for understanding the influence of the experimental parameters.

Equivalent Loading to Wave Action

The wave action on a cylindrical structure can be computed under the following assumptions. We consider linear waves passing over a cylinder at rest (of small velocity compared with the flow velocity). Diffraction effects are neglected (i.e. the pipe diam is small compared with the wavelength) as well as vibrations and turbulent effects. The orbital velocity at the bottom is:

$$V = \frac{\pi H_w}{T \sinh(\lambda h)} \cos\left(\frac{2\pi t}{T}\right)$$

where H_w is the wave height, i.e. twice the wave amplitude, h is the water depth, T is the wave period and λ is the wave number, such that:

$$\lambda \tanh(\lambda h) = \frac{4\pi^2}{gT^2}.$$

The empirical Morison (1950) equation (e.g. Sumer and Fredsøe, 1997) defines the in-line force due to wave action:

$$F_h = \frac{1}{2}\rho C_D D V|V| + \rho C_M \frac{\pi D^2}{4}\dot{V}$$

where C_D and C_M are functions of the Keulegan-Carpenter number (Bryndum et al., 1992). Fig. 3 shows a solution of this equation for a 1.5-m-high linear wave and a 2-m water depth. For such a large wave, close to breaking conditions, the linear assumption of the model is certainly a shortcoming. Still, the forcing could also schematically represent the wave-induced cyclic effects on a floating structure, transmitted to flow lines or risers resting on a deeper seabed.

Fig. 4 gives an example of the force measured on the pipe against its displacement. The plot of the measured force is similar to that shown in Fig. 3, but more peaked. We note that the maximum displacement is reached when the force is maximum. The smoother variation in the force as the orbital velocity is close to zero in Fig. 3 is approximately reproduced in our experiments.

Sand Characteristics

The Fontainebleau sand used in the tests is a naturally occurring, uniform, fine silica sand with sub-rounded grains of Tertiary marine origin. It is remarkably pure, with 95% silica. It has been widely used as a so-called standard academic sand in French geotechnical laboratories. Its main physical characteristics are: $D_{50} = 0.156$ mm, $C_u = D_{60}/D_{10} = 1.47$, $D_{60} = 0.168$ mm, $D_{10} = 0.114$ mm, $e_{\max} = 1.06$, $e_{\min} = 0.55$, $\gamma_{\min} = 12.87$ kN/m^3, $\gamma_{\max} = 17{,}23$ kN/m^3, $\gamma_s = 26{,}5$ kN/m^3. The permeability has a value of 10^{-5} m/s for dense sand and 1.5×10^{-5} m/s for loose sand.

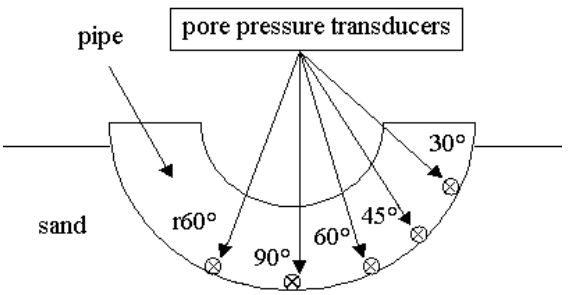

Fig. 2 Distribution of pore-pressure transducers along pipe-soil interface

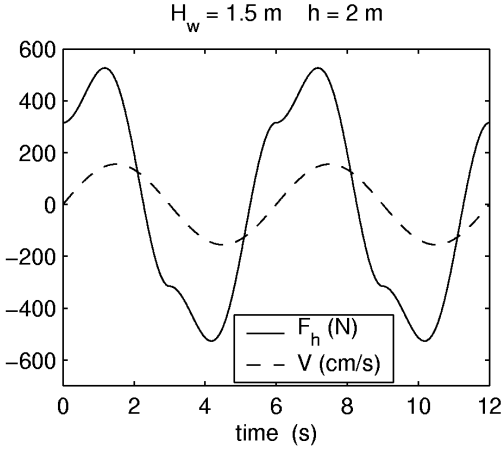

Fig. 3 In-line force obtained from Morison equation (F_h) against flow velocity at bottom (V)

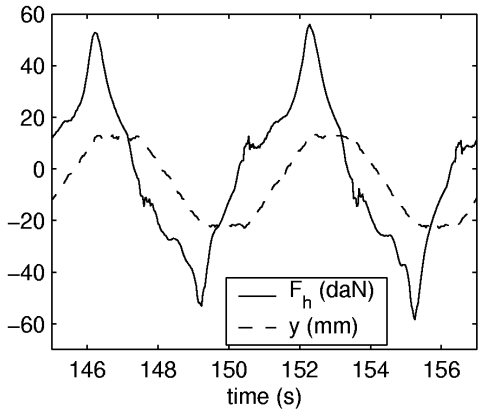

Fig. 4 Measured horizontal force (F_h; 1 daN = 10 N) against horizontal displacement (y)—load-controlled test L8

TESTING PROCEDURE

Sandbed Preparation

Three methods were used to prepare sand beds: dry pluviation followed by saturation of the tank; pluviation of the sand above the water surface; and pluviation through the water followed by vibration of the soil.

Dry method, loose sand. A dry pluviation system is used to deposit the sand from a low drop height. The lower the drop, the looser the sand arrangement will be. This method produced quite loose sand, with a density index I_D of about 35%. Once all the sand required is in place, a very low uplift gradient is applied at the bottom of the tank. This low gradient is more likely to let the water push away all air bubbles in the sand, instead of keeping them captive. A gravel layer previously installed on the tank bottom and covered by a geotextile membrane ensures a uniform distribution of the hydraulic gradient over the tank surface and homogeneous saturation of the sand. Good saturation of the sand mass was obtained through this method. After filling the tank with water, the water table is kept at a level of about 10 cm above the sand surface to ensure it will remain saturated during the movement of the pipe.

Wet method, medium-dense sand. Denser sandbeds are prepared by vibrating initially loose sand with a vibratory rod. The vibration process is performed while keeping the sand saturated. The density index obtained by this procedure was about 60%.

Wet method, loose sand. In order to perform more tests, not all the sand is removed, dried and then set back in the tank between each test. To reproduce the loose seabed, only the dense sand is removed, and then poured back by pluviation above the water surface. This procedure again produces a loose sand mass, whose density was found to be very similar to that obtained by the dry method.

The homogeneity of the sandbed and its density were controlled by performing light dynamic penetrometer tests using a small-diam rod.

TESTING PROGRAM

Tables 1 and 2 summarize the tests performed.

Load-controlled Tests (Table 1)

For each test, the horizontal cycles were applied after the vertical pipe penetration under its self-weight, starting from the sand surface. In these series, the experimental parameters explored were the load amplitude (30 to 90 daN), the loading period (2 s to 8 s), and the relative density of the sand (35% and 60%). During the tests, cyclic horizontal displacements were recorded together with vertical pipe penetration and pore pressures around the structure.

Test Number	Density Index (%)	Period (s)	Load Amplitude (daN)
L1	35	4	50
L2	35	2	50
L3	60	4	50
L4	60	2	50
L5	60	4	30
L6	60	4	60
L7	60	6	90
L8	60	6	60
L9	60	8	60
L10	60	6	30
L11	35	6	60

Table 1 Load-controlled testing program

Displacement-controlled Tests (Table 2)

These tests cover basically the same experimental parameters. Periods from 1 s to 6 s were studied in the tests performed with the actuator, and a constant period of 15 s was applied for the tests with the eccentric sinusoidal movement. Amplitudes of the applied lateral displacements of the pipe varied from 10 mm to 80 mm. The corresponding change in lateral force was recorded.

PIPE PENETRATION UNDER CYCLIC LOADING

Influence of Loading Period

Fig. 5 represents the increase in vertical pipe penetration with the number of loading cycles for tests in dense sand with a force amplitude of 60 daN and loading periods of 4, 6 and 8 s. The highest penetration is observed for the shortest period, and little difference is noted between the curves corresponding to 6 s and 8 s. This result has to be compared with the changes in maximum excess pore pressure measured during each cycle along the pipe and represented in Fig. 6: The highest values of the pore pressure are obtained for the shortest period. This suggests that the short period corresponds to loading conditions close to undrained ones, and that partial drainage occurs for periods of 6 s and 8 s. The drainage conditions are related to the horizontal velocity of the pipe with respect to sand permeability.

Test Number	Density Index (%)	Period (s)	Displacement Amplitude (mm)
D1*	60	6	52
D2*	60	2	10
D3*	35	1	5
D4**	35	15	40
D5**	35	15	60
D6**	35	15	80

*performed with actuator set
**performed with motor set

Table 2 Displacement-controlled testing program

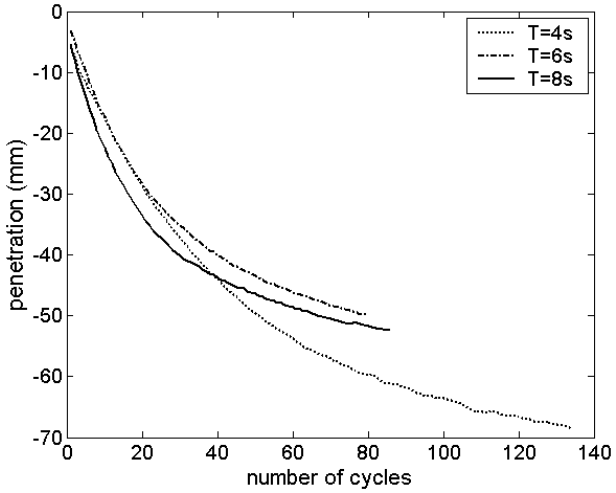

Fig. 5 Influence of loading period on pipe penetration—60 daN maximum applied load, dense sand

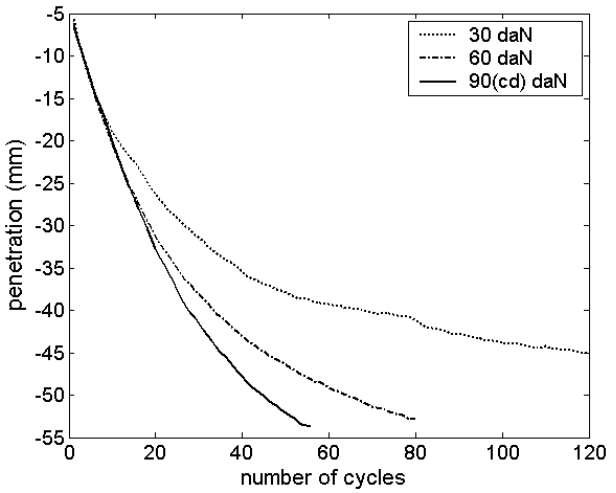

Fig. 7 Influence of load amplitude on pipe penetration—$T = 6$-s period, dense sand

In fact, because of the regulation system used to control the actuator movements, if the period is short, the actuator has very little time to reach its prescribed value, thus needing to move much faster. In contrast, over a long period the actuator does not need to move as fast to mobilize the prescribed resistance of the soil. Thus, the increase in peak pore pressure values is in close relation to the velocity of the actuator. For a given load, the shorter the period, the faster the pipe moves, and the higher the maximum pore pressure generated because of a more undrained behavior. Again, greater penetration corresponds to the highest pore pressure values.

Influence of Load Amplitude

Fig. 7 shows the increase in pipe penetration as a function of time for a given period of 6 s and for 3 load amplitudes of 30, 60 and 90 daN.

The value of 90 daN is close to the maximum horizontal resistance of the pipe in static conditions, and it is logical to find greater pipe penetration for a higher load amplitude. The same corresponding trend is observed in the excess pore pressures at the pipe-soil interface in Fig. 8: The lower pore pressure corresponds to the lowest load. The tests confirm that greater penetration and excess pore pressure are obtained when loading conditions are close to undrained conditions.

All these tests suggest that the increase in pore pressure observed during each loading cycle is one of the key factors for pipe penetration and consequently its loss of stability.

Cyclic Load-displacement and Load-penetration Curves

Fig. 9a presents typical cyclic load-displacement loops for a load-controlled test (L8), and Fig. 10 for a displacement-controlled one. Despite some scatter in the experimental data, they show a very similar shape. For a similar load level, the displacement amplitude governs loop inclination.

Fig. 9b presents the trajectories followed by the pipe for the corresponding cyclic loops of Fig. 9a. It can be verified that maximum penetration occurs when the pipe is in the central part of the trench, within the soil zone smoothed by the liquefaction and erosion process.

The pipe-soil lateral stiffness can be determined by drawing a straight line joining the strength peaks (Fig. 10). A remarkable

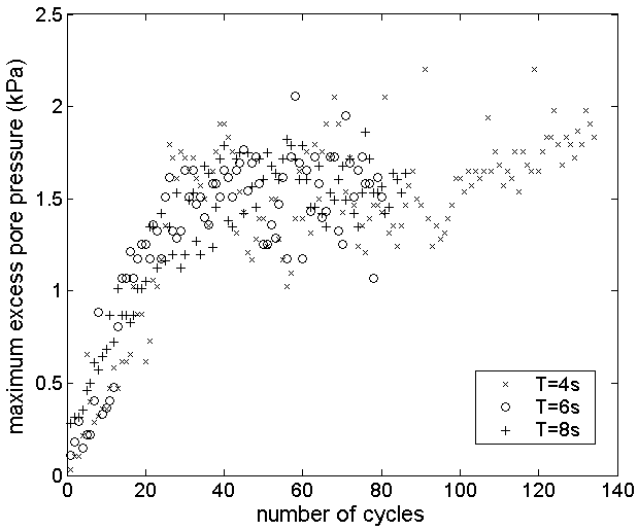

Fig. 6 Influence of loading period on excess pore pressure at 60° under pipe—60 daN applied force amplitude, dense sand

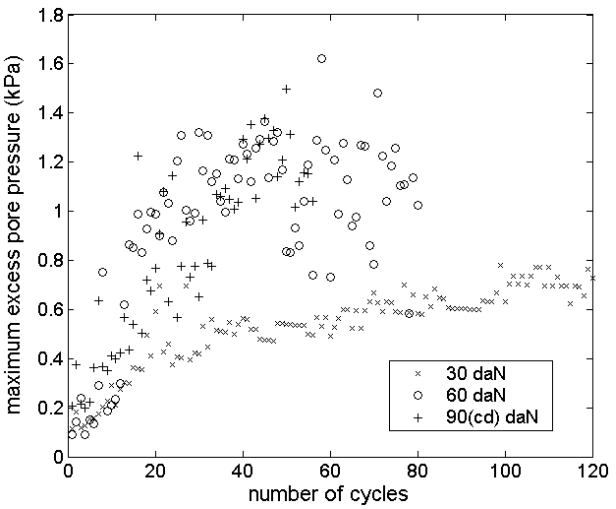

Fig. 8 Influence of load amplitude on maximum excess pore pressure at 60° during each cycle—6-s period, dense sand

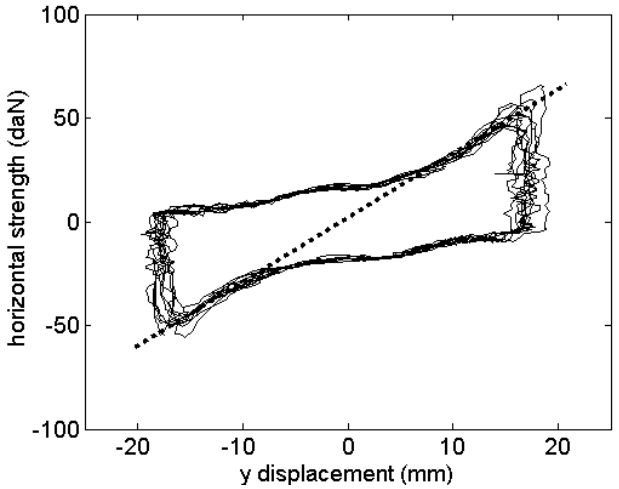

Fig. 9a Cyclic load-displacement curves for Test L8: 60 daN load amplitude, $T = 6$-s period

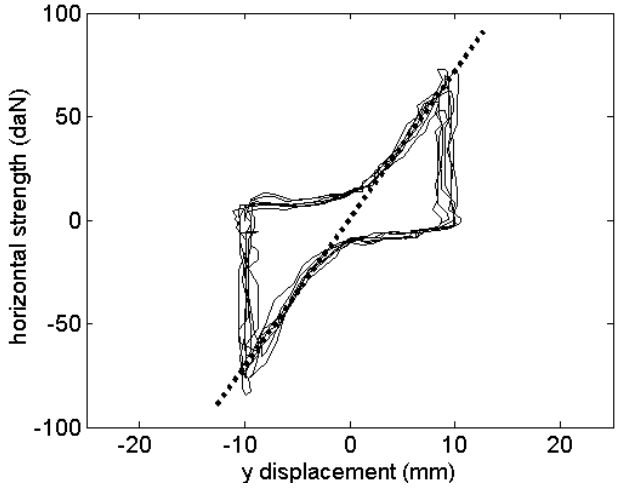

Fig. 10 Cyclic load-displacement curves for displacement-controlled Test D2: 10-mm amplitude, 2-s period

linear and symmetrical response of the loading stage of the pipe can be observed, with stiffness values of 7 daN/mm, in Fig. 10 and of 3 daN/mm in Fig. 9a. A very stiff unloading stage corresponds to the change in loading direction.

GENERATION OF PORE PRESSURE AT PIPE-SOIL INTERFACE AND LIQUEFACTION

Pore Pressure Recording Analysis

Excess pore pressure generation. Fig. 11 presents an example of the changes in peak excess pore pressure values measured by the transducer at 60° along the pipe. Also plotted were the corresponding values of the vertical effective stress at the same depth, assuming that $\sigma'_v = \gamma' \times z$ where γ' is the submerged weight of the sand and z is the depth. According to classical liquefaction analysis, the excess pore pressure needed to liquefy the sand should be equal to and not exceed the value of σ'_v. It may be noted that, during every cycle, the excess pore pressure reaches a much higher value than the vertical effective stress. This is certainly due to the fact that, during the lateral pushing of the pipe against the trench sides, the soil close to the pipe follows a more complicated undrained stress path. Using the simplified model developed by Branque et al. (2002), the passive pressures mobilized along the pipe surface at the level of the pore-pressure transducer (60°) could be calculated. In the case of the present experiments, they were found to be in the order of 6 kPa, obviously much higher than σ'_v. The values of the peak pore pressures are intermediate between the passive pressure and σ'_v. This indicates that the practical liquefaction criterion is conservative in this loading case due to the complicated stress path around the pipe. An intermediate stress between passive pressure and σ'_v, or the mean effective stress p', would be more appropriate.

The complete history of the cyclic changes in excess pore pressure represented in Fig. 12 indicates that the maximum excess pore pressure value increases with the number of cycles at the beginning of the loading, but that it tends to stabilize after a few cycles, although the pipe continues to sink. This confirms that a critical pore pressure value exists, corresponding to the initiation of liquefaction, which cannot be exceeded.

Pore pressure changes during cycle. Fig. 13 shows the changes in excess pore pressure with the horizontal displacement during

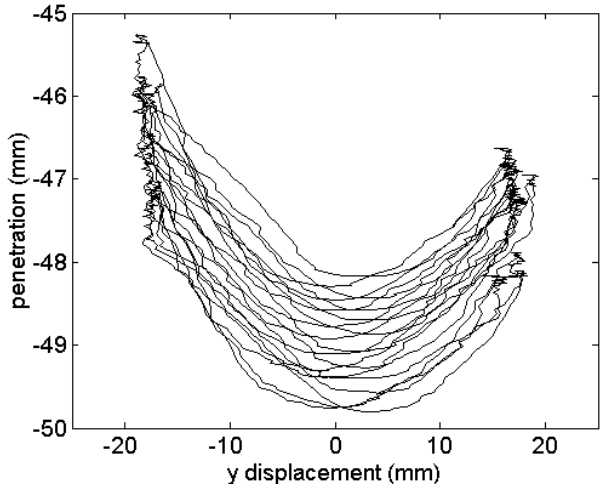

Fig. 9b Cyclic penetration-displacement curves of pipe (Test L8)

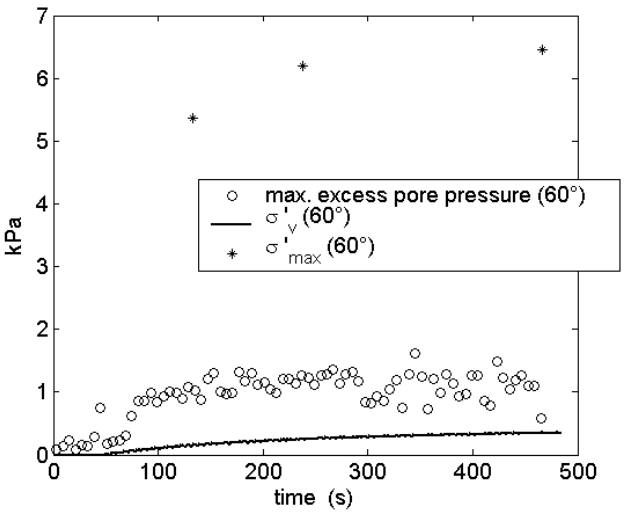

Fig. 11 Excess pore pressure at 60° under pipe compared to effective vertical stress and passive pressure stress at same depth—load-controlled test L8: 60 daN load amplitude, $T = 6$-s period

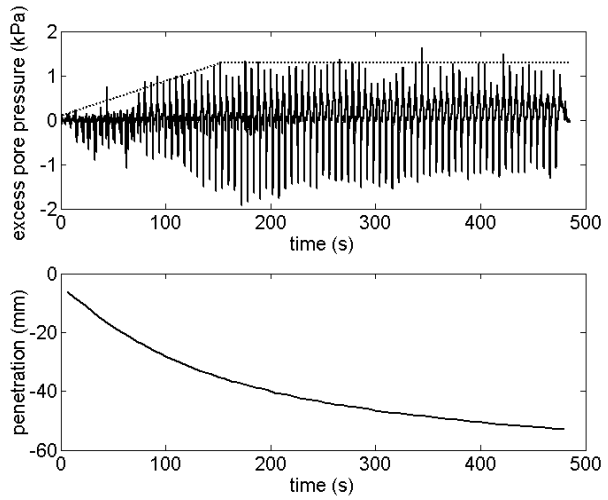

Fig. 12 Load-controlled test: 60 daN amplitude, $T = 6$-s period, dense sand

the cycles. The graph corresponds to the transducer on the right of the pipe, which explains the asymmetrical shape of the cyclic loops. As shown in Fig. 12, strong depressions are measured each time the pipe changes direction and lifts off the trench side. The absolute value of the depression is greater than the excess pore pressure generated during the loading stage.

When the horizontal displacement y of the pipe increases, it moves towards the pore-pressure transducers. These are in contact with the trench side for the higher values of y, and the pore pressure increases when the pipe pushes against the trench side. Slight drops in pressure also occur just before the maximum displacement, however, when y is still increasing. This might correspond to the moment when a critical pore pressure level is reached, and the sand liquefies. This liquefied layer is then pushed off the trench by the pipe, causing large displacements, high shear stresses and dilatancy of this part of the sand. The increasing pore volume may cause the observed drop in pressure.

Pore pressure distribution along the pipe. The maximum amplitude of the pore pressure measured around the pipe is at 60°

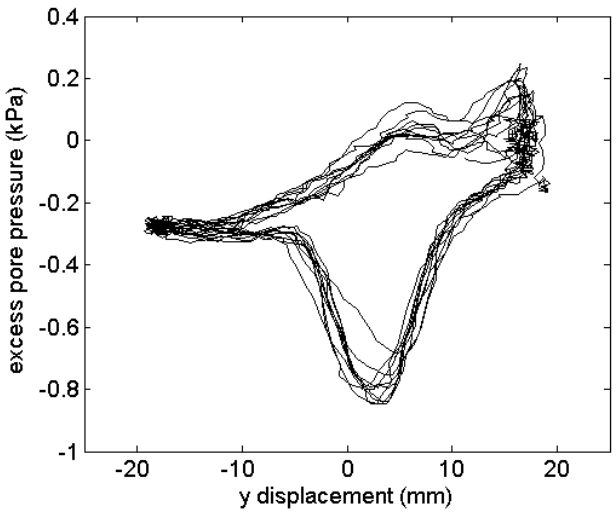

Fig. 13 Cyclic pore pressure changes at pipe-soil interface (transducer at 60°) during Test L8

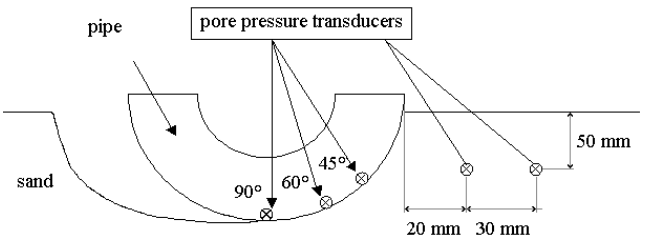

Fig. 14 Location of pore-pressure transducers along pipe and in soil

beneath the horizontal. The phenomena recorded at 45° are less important. However, the level reached by the excess pore pressure (about twice the effective vertical stress) seems great enough to liquefy the soil at this location. On the other hand, the transducer set right under the pipe (90°) did not measure any excess pore pressure, certainly due to the vicinity of the open trench behind the pipe. The one at 30° measured only very low variations in the pore pressure level, possibly due to drainage occurring close to the sand surface. In fact, the most significant pore pressure activity occurred in the range between 45° and 90°. The transducer set on the other side of the pipe recorded pressure data very similar to its symmetrical counterpart (60°). This confirms that instrumentation of one side of the pipe is sufficient in the present case to monitor the whole burial process.

Pore Pressure in Sandbed Close to Pipe

A series of tests was performed with 2 pore-pressure transducers within the soil (Fig. 14). The transducers were buried at a depth equal to half the maximum penetration allowed for the pipeline, and their minimum distances to the pipe were, respectively 20 and 50 mm.

Fig. 15 shows the changes in excess pore pressure measured by the 2 transducers within the soil. The qualitative changes in pore pressure measured at the pipe-soil interface are reproduced with an attenuation according to the distance to the pipe.

The transducers show that, even within the soil, suction is felt when the pipe lifts off the trench side. During each cycle, absolute depression peak values remain greater than the value of the excess pore pressure generated. Thus, no general buildup is measured

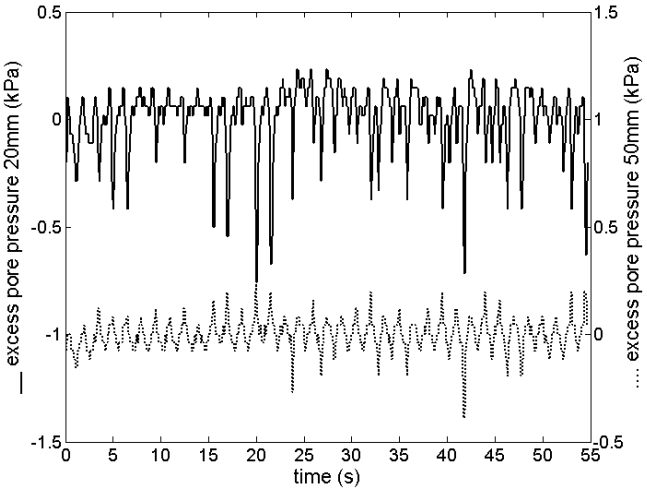

Fig. 15 Recording from pore-pressure transducers within soil: Displacement-controlled Test D2, performed with electromechanical actuator set, $T = 2$-s period

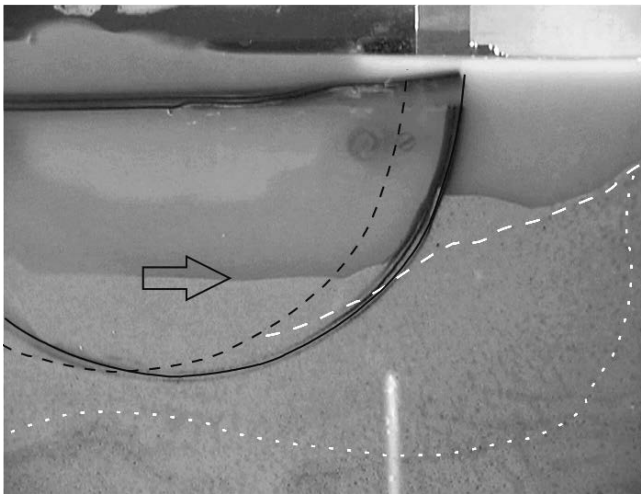

Fig. 16 Video frame at maximum excursion of pipe (load-controlled Test L4, maximum applied horizontal force: 50 daN, $T = 2$ s). Black and white dashed line = pipe position and soil/water interface at preceding half-period. Grain mobility area bounded by dotted line (motions over last half-period).

during the burial of the pipe, since the residual pore pressure level after any cycle is always the hydrostatic level.

Visualization of Liquefaction

Some tests were videotaped for accurate analysis of the seabed strains around the pipe during burial. Fig. 16 gives a video-frame example. It is obvious from these videos that a thin layer of sand close to the pipe behaves like a liquid. It flows away from the trench when the pipe moves towards the bank, and then flows under the pipe when it lifts off backwards. It is also noticeable that a significant volume of the sand in front of the pipe is submitted to large strains. The dotted line approximately defines the extension of this so-called plastic zone. No general liquefaction of the sandbed was observed .

Similar deformation patterns were recorded in most of the tests performed. In the tests with a large amplitude, an open trench was developed behind the pipe.

CONCLUSIONS

The first test results show a strong pore pressure increase at the pipe-soil interface during the horizontal loading of the pipe.

This increase is sufficient to induce instantaneous liquefaction at each cycle in a layer close to the pipe wall.

This paper presents only those results obtained with dense sand, but all the tests performed indicate that the increase in pore pressure and pipe penetration depends on soil density, load amplitude and loading period. Further investigations are still needed to explore the influence of the different parameters, but a key factor seems to be the actuator velocity with respect to the soil permeability, leading to more or less undrained loading conditions.

Direct visualization of the self-burial process clearly showed the liquefaction phenomenon. This local and transitory liquefaction plays an important role in the burying of the pipe and its loss of stability. However, due to the depression during the unloading stage, no general liquefaction of the sandbed was induced by the cyclic movement of the pipe. This point confirms the difference between the response of the sandbed by itself and when it interacts with a cyclically loaded structure.

While the conditions of pore pressure generation are beginning to be well understood, a good reference pore pressure level linked to the initiation of liquefaction remains to be determined. The classical liquefaction criterion using the effective vertical stress is not relevant in this case.

ACKNOWLEDGEMENTS

This study was partially funded by the European Commission Research Directorate, FP5, specific program “Energy, Environment and Sustainable Development,” Contract No EVK3-CT-2000-00038, Liquefaction Around Marine Structures (LIMAS).

REFERENCES

Branque, D (1998). “Etude de l’Auto Ensouillement des Pipelines Flexibles Soumis à la Houle et aux Courants Marins,” *PhD Dissertation*, Institut National Polytechnique de Grenoble, 397 pp.

Branque, D, Foray, P, and Labanieh, S (2001). “Etude Expérimentale de l’Interaction entre les Fonds Marins et les Pipelines Flexibles Soumis à la Houle et aux Courants," *Revue Française de Géotechnique*, Vol 97, pp 61–78.

Branque, D, Foray, P, and Labanieh, S (2002). “Wave-induced Interaction Between Soil and Flexible Pipelines Resting on the Seabed,” *Physical Models in Geotechnics, Proc Int Conf Phys Modelling in Geotechnics*, St John, Newfoundland, Balkema Pub, pp 271–276.

Brennoden, H, Sveggen, O, Wagner, DA, and Murff, JD (1986). “Full Scale Pipe-soil Interaction Tests,” *Proc 18th Offshore Tech Conf*, OTC 5338, Houston.

Bryndum, MB, Jacobsen, V, and Thasalis, DT (1992). “Hydrodynamic Forces on Pipelines: Model Tests,” *J Offshore Mech and Arctic Eng*, ASME, Vol 114, pp 231–241.

Cheng, L, Sumer, BM, and Fredsøe, J (2001). “Solutions of Pore Pressure Buildup Due to Progressive Waves,” *Int J Num and Analyt Meth in Geomech,* Vol 25, pp 885–907.

Damgaard, JS, and Palmer, AC (2001). “Pipeline Stability on a Mobile and Liquefied Seabed: A Discussion of Magnitudes and Engineering Implications,” *Proc Conf Offshore Mech and Arctic Eng*, Rio de Janeiro; no page range given.

Lambrakos, KF (1985). “Marine Pipeline Soil Friction Coefficient from In-situ Testing,” *Ocean Eng*, Vol 12, No 2, pp 131–150.

Lyons, CG (1973). “Soil Resistance to Lateral Sliding of Marine Pipelines,” *Proc 5th Offshore Tech Conf*, OTC 1876, Houston.

Morison, JR, O’Brien, MP, Johnson, JW, and Schaaf, SA (1950). “The Forces Exerted by Surfaced Waves on Piles,” *J Petro Trans*, AIME, Vol 189, pp 149–154.

Morris, DV, Webb, RE, and Dunlap, WA (1988). “Self-burial of Laterally Loaded Offshore Pipelines in Weak Sediments,” *Proc 20th Offshore Tech Conf*, OTC 5855, Houston.

Palmer, AC, Steenfelt, JS, and Jacobsen, V (1988). “Lateral Resistance of Marine Pipelines on Sand,” *Proc 20th Offshore Tech Conf*, OTC 5853, Houston.

Sassa, S, Seikiguchi, H, and Miyamoto, J (2001). “Analysis of Progressive Liquefaction as a Moving Boundary Problem,” *Géotechnique*, Vol 51, No 10, pp 847–857.

Sumer, BM, and Fredsøe, J (1997). *Hydrodynamics Around Cylindrical Structures, Adv Series on Ocean Eng*, Vol 12, World Scientific.

Sumer, BM, Fredsøe, J, Christensen, S, and Lind, MT (1999). "Sinking/flotation of Pipelines and Other Objects in Liquefied Soils Under Waves," *Coastal Eng*, Vol 38, pp 53–90.

Sumer, BM, Hatipoglu, F, Fredsøe, J, and Ottesen Hansen, N-E (2005a). "Critical Flotation Density of Pipelines in Soils Liquefied by Waves," submitted for publication in *ASCE J Waterways, Port, Coastal and Ocean Eng*.

Sumer, BM, Truelsen, C, and Fredsøe, J (2005b). "Liquefaction Around Pipelines Under Waves," submitted for publication in *ASCE J Waterways, Port, Coastal and Ocean Eng*.

Teh, TC, Palmer, AC, and Damgaard, JS (2003). "Experimental Study of Marine Pipelines on Unstable and Liquefied Seabed," *Coastal Eng*, Vol 50, pp 1–17.

Wagner, DA, Murff, JD, and Brennodden, H (1987). "Pipe-soil Interaction Model," *Proc 9th Offshore Tech Conf*, OTC 5504, Houston.

Wolfram, WR, Getz, JR, and Verley, RLP (1987). "Pipestab Project: Improvement Design Basis for Submarine Pipeline Stability," *Proc 19th Offshore Tech Conf*, OTC 5501, Houston.